On regional differences in the seasonality of northern hemisphere temperature

Bachelorarbeit im Studiengang Physik des Erdsystems (BSc)
an der Christian-Albrechts-Universität zu Kiel

vorgelegt von:

Felix Schreyer

1. Gutachter: Prof. Dr. Richard Greatbatch
2. Gutachter: Dipl. Met. Gereon Gollan

Kiel, Juli 2014

Contents

Abstract

Regional patterns in the seasonality of temperature were investigated in the extra-tropical northern hemisphere by analysing amplitude and phase of the annual cycle based on ERA-Interim reanalysis data. Besides the dominant contrast between continental and maritime climate, regional anomalies in temperature seasonality were detected over northern North America and northern central Asia. The signal is most pronounced over Canada east of the Rocky Mountains, where an anomalous delayed annual cycle can be observed.

Analysis of sea level pressure (SLP) and 500 hPa geopotential height (z500) fields shows distinctive differences in spring and autumn mean circulation that are largely consistent with the deviating annual cycle phases in those regions. Northeastern North America for instance is exposed to more cold maritime northeasterly influence in spring and a more warm continental southwesterly circulation in autumn. EOF-Analysis of SLP anomalies poleward of 20°N indicates two patterns, constituting the spring-autumn asymmetries in surface flow. The first EOF captures an equivalent of the Cold-Ocean-Warm-Land pattern (COWL) for SLP, describing seasonal contrasts between continental high pressures and oceanic low pressures. It is found to have an annual cycle that is about one month earlier than the average temperature annual cycle on the northern hemisphere. The second EOF is similar to the Northern Annular Mode (NAM), but includes an interseasonal polarity of the transition seasons, indicating enhanced westerlies in autumn. The same argument can be made for the jet stream by conducting EOF-Analysis of the z500 field. 500 hPa flow components and momentum fluxes are furthermore analysed that confirm a stronger and northward shifted jet stream in autumn relative to spring. Planetary stationary wave patterns are additionally found to be centered more westward in autumn with characteristic southwestward extensions. This suggests a link between the discussed seasonal circulation changes and the jet stream features in spring and autumn due to different orographic forcing of stationary waves in the two seasons.

---

1 Introduction

The annual cycle is the main component of climate variation in the extratropical latitudes. Due to the tilting of the Earth's rotation axis the hemispheres are exposed to different levels of solar insolation in winter and summer, leading to a distinctive seasonality in local temperature. Its main characeristics can be described by the ampltiude and phase of the annual cycle obtained by harmonic analysis. The amplitude stands for the range of annual temperature variation, whereas the phase expresses the time lag of the temperature signal behind the solar cycle. Applying this method reveals distinctive regional differences in seasonality beyond latitudinal position only. It is mainly the land-sea constrast in heat capacity and the dynamic atmospheric circulation that influence the annual cycle of local temperature. Since land areas heat and cool much quicker than the ocean, continental seasonality is normally associated with high amplitudes and early phases. On the other hand, low amplitudes and late phases reflect maritime climate. This has been well-known for a long time and was already investigated by *Kendrew* (1927) as well as *Prescott and Collins* (1951). *White and Wallace* (1978) noted that in midlatitudes this temperature seasonality is obviously advected eastwards, implying that western continental margins have a more martitime annual cycle than their eastern counterparts. Recently, *Stine et al.* (2009) calculated a local "seasonal response index", which is based on the difference between normalised annual cycle amplitude and phase, and found 75% of its spatial variance explained by the distance to the nearest western coast.

In the study presented here, regional differences in seasonality beyond this land-sea concept will be examined and connections to seasonal changes in circulation patterns will be drawn. It is therefore divided into two main parts: Firstly, regional patterns in seasonality will be documented with an improved spatial resolution on the basis of updated data products. Thereby, reanalysis as well as station data will be used. Secondly, an explanation for some observed anomalies in seasonality will be suggested by investigating spring-autumn contrasts in lower- and mid-tropospheric circulation.

Figure 1 depicts the surface temperature seasonal cycle at four stations at about 50°N latitude. The seasonal cycle is obtained by computing a daily climatology in temperature over the period from 1959 to 2009. The stations are situated at each side of the two continents close to the oceanic coast. Evidently, amplitude, phase and the annual mean vary to some degree across the four locations, even though their distance to the ocean and latitudinal position is practically the same. Of course, there are several other geographical factors, revealing this comparison to be rather oversimplified, but it nevertheless illustrates some aspects of the regional differences in seasonality in a first step. St John's (Eastern Canada) and Bogorodskoe (Eastern Russia) present

considerably higher amplitudes and lower annual means than their counterparts on the West. This can be easily related to the prevailing westerlies in these latitudes, exposing eastern continental margins to different temperature signals than western margins. Additionally, planetary stationary waves due to orographic forcing emerge in the winter NH and create troughs over northeastern North America and eastern Asia as well as ridges over Europe and northwestern North America as described by e.g. *McHall* (1991).

Examining the annual cycle phase in figure 1 requires a closer look and could be estimated by looking at the position of the maximum and minimum temperatures. It is noticeable that in particular at St John's in Newfoundland the seasons seem to start later than at the other places. Not only is there a sharp contrast to Bogorodskoe at the eastasian coast, the phase also seems to be later than in Vancouver or La Rochelle, where the influence of westerlies has to be considered. Interestingly, there are more stations in northeastern North America (not shown here), located further into the continent, which carry this signal of a delayed annual cycle as well. This stands in contrast to the general tendency of an eastward declining phase over the continents due to the westerlies as e.g. described by *White and Wallace* (1978) or *Stine et al.* (2009). In the study presented here, there will be a special focus on collecting evidence and explanation for a delay in seasonality over northeastern North America.

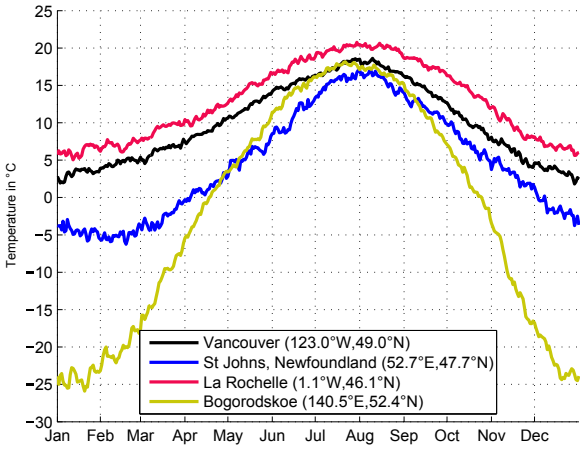

Figure 1: *Seasonal cycles of surface temperature at 4 different stations situated at continental margins in the midlatitudes. The seasonal cycle is obtained by averaging daily data over a period from 1959 to 2009. See appendix 5.1 for details on the station datasets.*

2 Data and Methods

2.1 Data

In order to examine the seasonal cycle characteristics on a well-resolved grid, reanalysis data from 1979 to 2013 provided by the ERA-Interim project of the European Centre for Medium-Range Weather Forecasts (ECMWF) are used. It is based on a 512×256 global Gaussian grid. In this study, daily data for 2m-air-temperature, 500 hPa geopotential height (z500) and 500 hPa zonal and meridional wind are analysed. Furthermore, sea level pressure (SLP) and downward solar radition flux is processed on a monthly basis.

The station data come from three different sources: The American continent is covered by the Global Historical Climatology Network of the National Climatic Data Center (NCDC, United States). For stations of this dataset not providing daily mean temperatures, the average of daily minimum and maximum temperature is computed. The other station data originate either from the European Climate Assessment and Dataset project (ECAM) or, for several locations in eastern Russia, from the Carbon Dioxide Information and Analysis Center at Oak Ridge based on *Bulygina and Razuvaev* (2012). For all stations the period from 1959 to 2009 is extracted. It has to be considered that daily station data over a 50 year period naturally involve gaps. To guarantee a certain data density, stations lacking more than 10% of the time series are removed. See section 5.1 in the Appendix for detailed information on the station data.

The core element in the analysis of seasonality is the temperature seasonal cycle. It is obtained from reanalysis as well as station data by averaging the local temperature of each day of the year from the time series over all years. To eliminiate possible warming signals of the annual mean temperature over the period averaged, the linear trend of the time series is removed beforehand. However, this last step seems to have negligible consequences for the resulting seasonal cycle, varying the temperature only in magnitude of 10^{-2}°C. The monthly climatology produced by this means shall hereinafter be referred to as the seasonal cycle.

2.2 Harmonic Analysis

The fundamental method to gain insight into seasonality is to conduct a harmonic analysis of the temperature seasonal cycle. The first harmonic has a yearly period and is referred to as the annual cycle. It is obtained in this study by fitting

$$AC(t) = -A\,cos(\frac{2\pi(t-\phi)}{p}) + m \tag{1}$$

to the seasonal cycle. Therein, t denotes the time in days referenced to the solar cycle (at Dec 21: $t = 0$), $A > 0$ the amplitude, ϕ the phase (day of annual cycle minimum), $p = 365\,d$ the period and m the annual mean temperature. The amplitude is always positive since only the northern hemisphere polward of 30°N is analysed, so that the annual cycle minimum is in boreal winter. The fitting routine treats A, ϕ and m as free parameters, numerically searching the least square sum of the residual. It should be noted that not all variance of the seasonal cycle can be explained by the annual cycle. The goodness of the fit can be seen in Figure 2 for the ERA-Interim data. Especially at high latitudes and over the oceans the semi-annual cycle ($p = 365/2\,d$ in (1)) can explain much of the residual variance (see Appendix section 5.2). For the ERA-Interim data annual and semi-annual cycle together accounts for more than 97% of the seasonal cycle variance at all extratropical NH grid points. *White and Wallace* (1978) note a pronounced semi-annual cycle in polar regions as well with a phase similar to the annual cycle. This phenomenon is referred to as the "coreless winter", indicating a sharp maximum and a broad minimum in the seasonal cycle due to ice-albedo-feedbacks at these latitudes. However, the present study focuses on the annual cycle and is particularly concerned with midlatitudes over the continents, where the semi-annual component is mostly small.

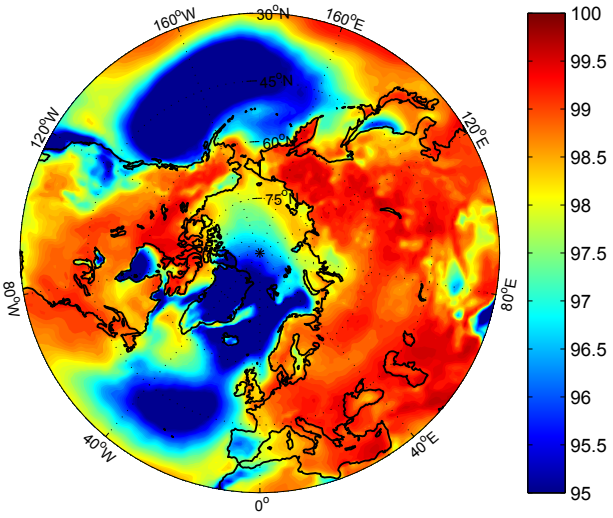

Figure 2: *Variance of seasonal cycle explained by the annual aycle in %. The seasonal cycle is a daily climatology of temperature over 1979 to 2013 based on ERA-Interim data.*

2.3 Season Definitions

Another way to analyse seasonality is to determine the timing of individual seasons in the course of the year. The transition seasons, spring and autumn, are of particular interest since the annual cycle is steepest in these periods, so that phase differences should be most apparent. The astronomical definition of summer and winter half year onset is based on the solar cycle and refers to the equinoxes on March 21 and September

21 respectively. Due to geometrical reasons it marks the day when the solar insolation cycle crosses its annual mean. In this study, this very definition is applied in the same way to the temperature seasonal cycle, marking mid-spring and mid-autumn. Depending on the subject investigated, it can be also useful to work with fixed barriers of temperature as indicators of seasons. Threshold responses in biological systems (plant growth, bird migration) as pointed out in e.g. *Schwartz et al.* (2006) or onsets of melting and freezing phases are captured by this means. Against this background the transition seasons can even be subdivided again. *Jaagus and Ahas* (2000) for example distinguish a "warm season" above 0°C, a "growing season" above 5°C and "summer" above 13°C. However, these fixed thresholds also depend on the background climate and therefore do not provide a useful reference for the large-scale annual cycle phase differences. A more appropriate way to complement the findings of the annual cyle analysis is rather to determine mid-spring and mid-autumn, defined by the day the temperature seasonal cycle stays above or below the annual mean respectively. To support this, correlation coefficients for all extropical NH land and ocean grid points are computed for annual cycle phase, mid-spring and mid-autumn. Annual cycle phase correlates with mid-spring and mid-autumn timing by 0.95 and 0.82 respectively. The latter mutually exhibit a correlation of 0.7. All correlations are significant.

Section 3.2 investigates differences in circulation between mean states of spring and autumn. The approach is closely related to the one of *Fleming et al.* (1987). It is not easy to say, which definition of spring and autumn mean state is most appropriate to trace differences in the flow field that can account for delays in the temperature annual cycle. There are several ways to define these seasons, which produce fairly different results when comparing circulation patterns. Since heating at the surface is the key forcing for the seasonaliy of all atmospheric processes, it appears reasonable to look for states of comparable tropospheric mean temperature. *Fleming et al.* (1987) computed annual cyles at different levels of geopotential height for the NH and found a quite uniform phase of 38 days behind solar cycle for levels between 700 hPa and 200 hPa. Accordingly, the transition seasons are centered on April and October 29, which is respected in the definition of the mean states as weighted averages (55%/45%) of April/May and October/November for spring and autumn. These definitions will be applied in section 3.2.

2.4 EOF-Analysis

EOF-Analysis is used to obtain time variability patterns for monthly anomalies over the period from 1979 to 2013 of sea level pressure (SLP) and 500 hPa geopotential height (z500) on the NH poleward of 20°N. The linear trend over time is removed and

anomalies relative to the climatological mean state are computed. Note that the seasonal cycle is not removed from the field as normally done for capturing interannual modes as principal EOFs. The anomalies are area-weighted with the square rooted cosine of the latitude to respect the poleward increasing grid point density. Subsequently, the covariance matrix of the anomaly field is computed and the first three Empirical Orthogonal Functions (EOF) are obtained by determining the eigenvectors with the highest eigenvalues. The principal component of each EOF is determined by projecting the original anomaly field onto the respective EOF pattern. The time series is then normalised to have zero mean and unit standard deviation. Finally, the eigenvalue corresponding to an EOF normed by the sum over all eigenvalues represents the fraction of explained variance by this EOF pattern. For a more detailed description of EOF-Analysis see e.g. *Bjornsson and Venegas* (1997) or *Hannachi and Jolliffe* (2006).

3 Results

3.1 Surface Temperature Seasonality

3.1.1 Annual Cycle Analysis

In Figures 3 and 4 amplitude and phase of the 2m-air-temperature annual cycle are presented for land areas in the extratropical NH. The amplitude is weighted by the zonally constant solar insolation amplitude, normalised to the 30°N latitudinal belt. Hence, the amplitude weight increases equatorward according to the solar insolation amplitude and is one at 30°N. This procedure removes the effect of latitudinal variation due to solar insolation, while keeping the unit of temperature (see appendix 5.3 for unweighted amplitude). The annual cyle phase is expressed as the lag behind the solar cycle (minimum on December 21).

Firstly, the general contrast of continental and maritime climate as discussed in section 1 can be observed: Inside the continents high amplitudes and early phases prevail. Regions with coastal influence exhibit low amplitudes and late phases. In midlatitudes the impact of the westerlies is apparent, leading to a more extensive maritime signal in central North America west of the Rocky Mountains and over western parts of Europe. Amplitudes are highest in continental subpolar regions, where a seasonal change in surface albedo adds to the temperature range. Maxima up to 18°C (32°C without weighting) are observed over eastern Siberia. Phases are earliest in some areas of central Asia, reaching down to only about 18 days in lag.

Yet, on closer inspection the distribution of annual cycle phase in Figure 4 reveals some interesting features, which cannot simply be attributed to continental and maritime heating contrasts. Phases are remarkably late over northeastern North America on both sides of Hudson Bay and this signal seems to extend even to central parts of the continent to latitudes of roughly 45°N. On the eastern side of Asia no such phase delay can be observed. Moreover, a sharp transition seems to prevail at the western Pacific coast with early phases occuring close to the continental margin. The annual cycle over northeastern North America is even more delayed than over large parts of Europe or western North America, where westerlies carry the maritime temperature signal inland. Additionally, the late phases in this region are not connected with low amplitudes as in maritime conditions. In fact, the amplitude over North America seems to coincide widely with the typical continentality pattern as Figure 3 suggests. Smaller related features can be discovered on the Asian continent as well: On Taymyr Peninsula in northern central Russia and on the northeastern Russian Chukchi Peninsula west of the Bering Sea. An inverse anomaly is indicated over northwestern North America, where small amplitudes are associated with an early annual cycle.

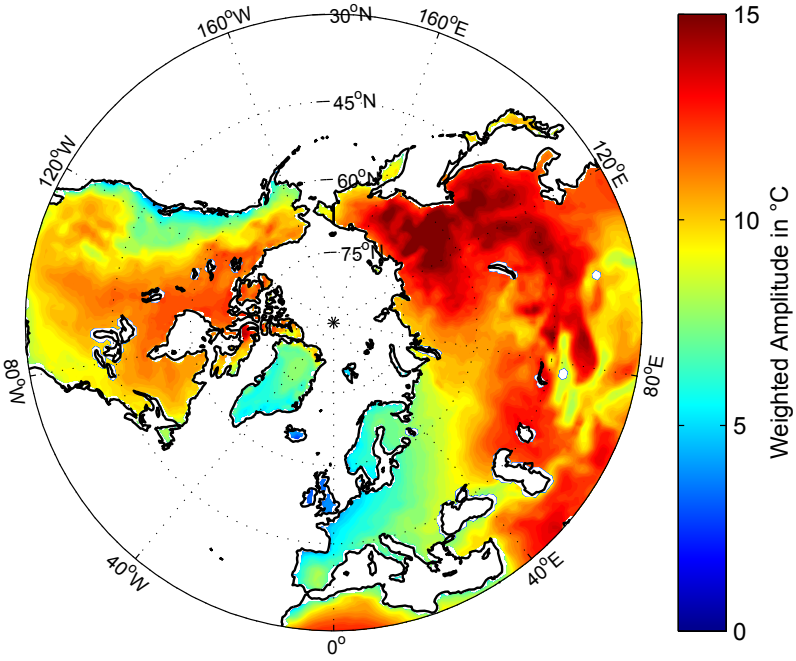

Figure 3: *Weighted amplitude $w \cdot A$ of 2m-air-temperature annual cycle in °C over the continents in the extratropical NH based on Era-Interim data. The weight is the solar cycle amplitude A_{sol} normed to 30°N latitude: $w = A_{sol}/A_{sol}(30°N)$. This removes the effect of the latitudinal increase in solar cycle amplitude. See appendix 5.3 for unweighted amplitude.*

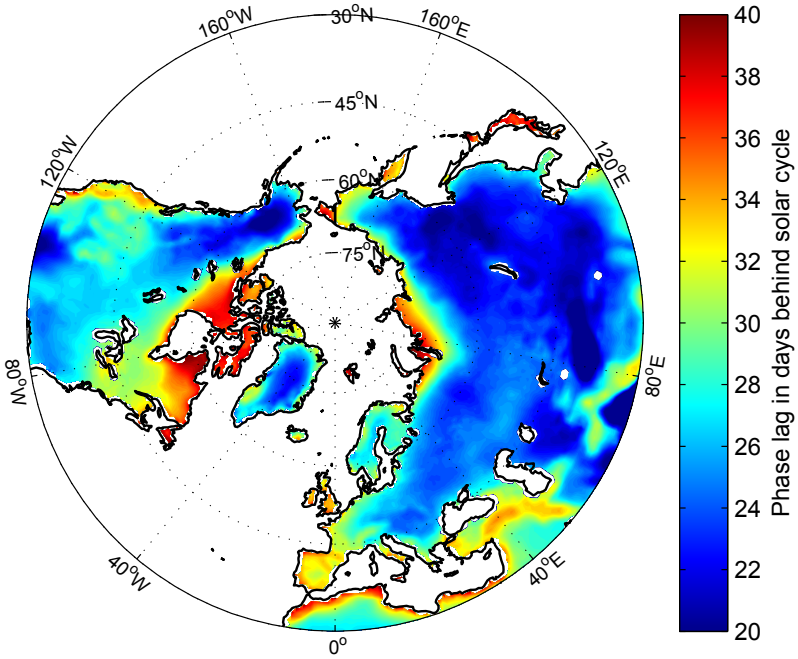

Figure 4: *Phase ϕ of 2m-air-temperature annual cycle in days behind solar cycle (minimum on December 21).*

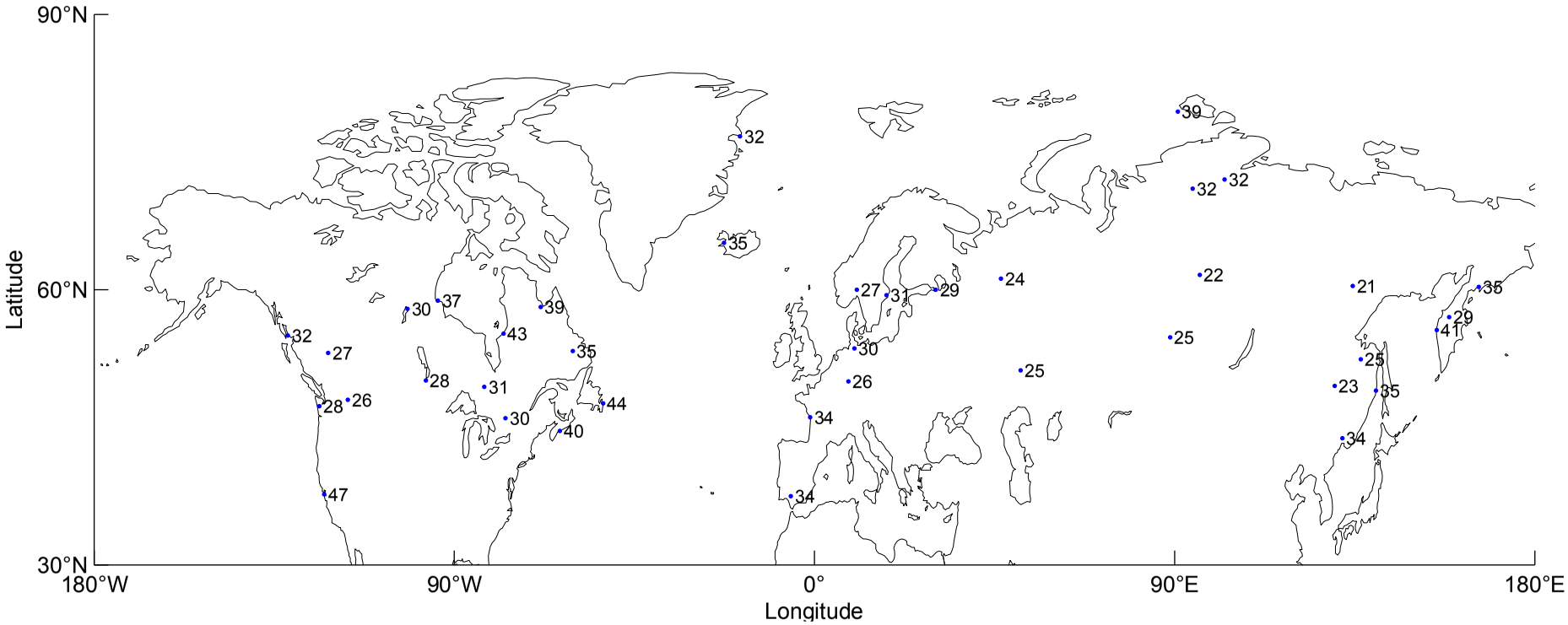

Figure 5: *Surface temperature annual cycle phase for several stations in the NH. The phase lag is defined as in Figure 4.*

Figure 5 shows annual cycle phases for several stations northward of 30°N. Even though the spatial data density is comparatively small, some features of Figure 4 can be reproduced. Looking at midlatitudes, northeastern North America exhibits later phases than northwestern North America. Furthermore, its annual cycle seems more delayed than over several parts of Europe and most of Asia. At the eastasian continental margin at about 50°N the station data also supports evidence of a sharp transition from continental to maritime phases. Finally, slightly delayed annual cycles are reproduced as well over the Taymyr Peninsula in Northern Russia.

However, care has to be taken when interpreting annual cycle analysis from station data since it obviously tends to provide results much less continuous than with grid point renalysis data. Consider for example two stations on Kamchatka Peninsula (Ica, Esso) or in northern central Canada (Brochet, Churchill, see station details in the Appendix 5.1), yielding a phase difference of 12 days and 7 days respectively between two very close locations. To validate method and findings of this station data analysis, a much better spatial resolution is needed.

Examining the distribution of grid points in the midlatitude NH in amplitude-phase space, Figure 6 illustrates the contrast of continental and maritime regions. *Stine et al.* (2009) assessed the observed arc structure in amplitude-phase-space to be a natural consequence of interacting land and ocean areas, whose seasonality can be mathematically described by two harmonics with different amplitude and phase. It can be understood as a mixing line, connecting continental and maritime seasonality. Moreover, they noted that the distance to the westward coast, where distance of ocean gridpoints is taken negative, generally declines down the arc. The spatial structure of seasonality can can primarily be understood with this concept of land-ocean heating contrasts and westerly advection. However, the observed late phases over northeastern North America do not go along with small maritime amplitudes and deviate from the mixing line as apparent in Figure 6. This cannot be explained by that approach. Another idea is to look for differences in spring and autumn circulation on the NH, which might influence the

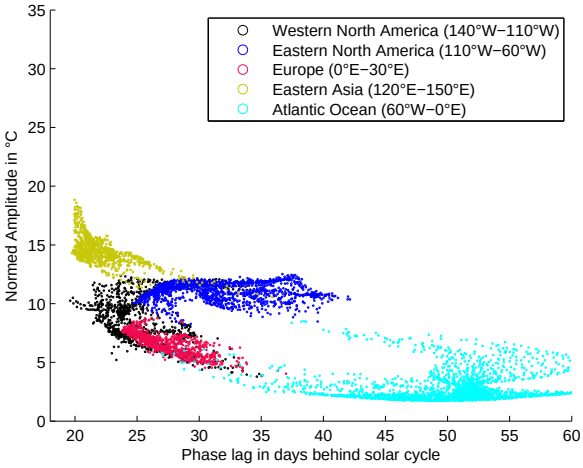

Figure 6: *Annual cycle amplitude-phase-space for several regions in the midlatitude NH (45°N-65°N). Amplitude is weighted and the phase is referenced to the solar cycle as in Figures 3 and 4.*

annual cycle phase in some regions. This will be discussed in further detail in section 3.2.

3.1.2 Spring and Autumn Timing

Motivated by the regional differences in annual cycle phase found in section 3.1.1 the timing of the transition seasons is examined using another approach. Figures 7 and 8 display mid-spring and mid-autumn based on the temperature seasonal cycle. Mid-Spring is defined as the day the seasonal cycle stays above annual mean temperature. The same applies to autumn when temperature stays below annual mean. Both dates are referenced to the respective equinox to express the lag behind the solar cycle.

Figure 7 reveals similiar patterns for mid-spring to those observed for annual cycle phase in Figure 4. Yet, the contrast between northeastern North America and Europe is less pronounced. Late springs only occur west of Hudson Bay. Northeastern North America however still experiences considerably later springs than eastern Asia. The signal of delayed seasons over northern and northeastern Russia observed in Figure 4 is also discernable in the shifted spring. In addition, particularly late crossings of the annual mean threshold can be observed on western continental margins at about 45°N. At higher latitudes in western Canada though, earlier springs occur as in comparable regions in Europe. In Figure 8 a pronounced signal of delayed autumn is noticeable over large parts of northeastern North America. There mid-autumns delayed by 43 days occur, whereas over the rest of the land areas this threshold is passed rather uniformly and earlier at about 25 to 30 days behind the solar cycle. Greenland is an exception, but the early autumns are connected with late springs there, indicating a long winter and a pronounced semi-annual cycle. Northeastern North America is the only region, where delayed springs and autumns occur together. Yet, compared to Europe the contrast seems most pronounced in the timing of autumn. The mid-spring and mid-autumn patterns discussed are also indicated by the station data (not shown here). Especially the anomalous autumn in northeastern North America and the advanced spring in eastern Asia can be well reproduced. Yet, as mentioned in section 3.1.1, there is less confidence in these station data results since comparatively high fluctuations occur within a region.

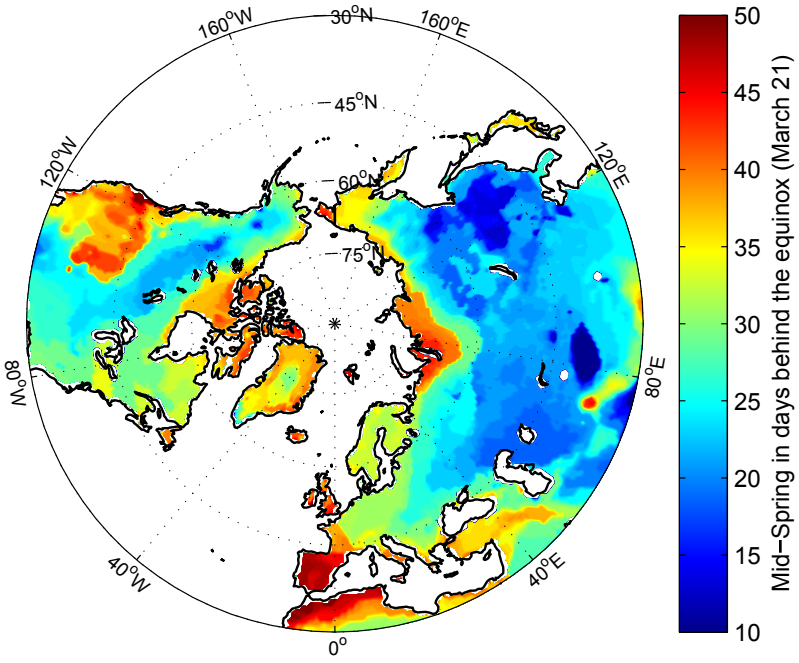

Figure 7: *Mid-Spring over the continents in the extratropical NH based on Era-Interim data. Mid-Spring is defined as day the seasonal cycle stays above the annual mean temperature. It is referenced to the solar cycle (March 21). The seasonal cycle is a daily climatology obtained by averaging over the period from 1979 to 2013.*

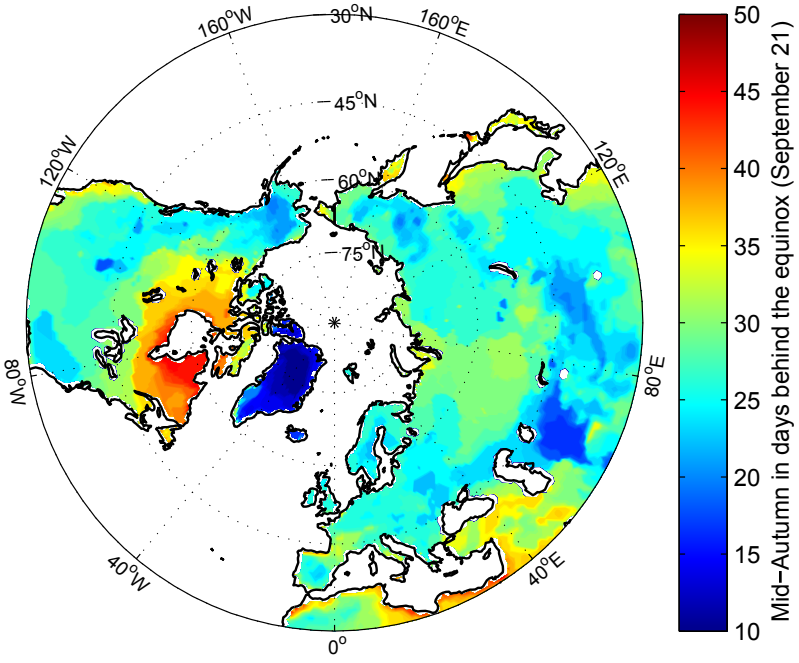

Figure 8: *As in Figure 7 except for autumn. Mid-Autumn is defined as day the seasonal cycle stays below the annual mean temperature. It is referenced to the solar cycle (September 21).*

3.2 Link to Seasonal Circulation Changes

Some regional anomalies in temperature seasonality were discovered in the previous section, which cannot be attributed to land-ocean heating contrasts alone. Especially the variation of annual cycle phase between midlatitude North America, Europe and Asia requires further explanation. Subsequently, seasonal circulation changes are discussed that might account for delayed season onsets in several areas. Differences in surface and 500 hPa flow between mean states of spring and autumn are analysed similiar to the approach of *Fleming et al.* (1987). This is done in order to see whether seasonal asymmetries in the circulation are linked to shifts in the temperature annual cycle phase. The following plots show the difference between spring and autumn, defined by weighted averages (55%/45%) of April/May and October/November based on a monthly climatology over 1979 to 2013, for SLP, z500 as well as 500 hPa flow components and momentum flux.

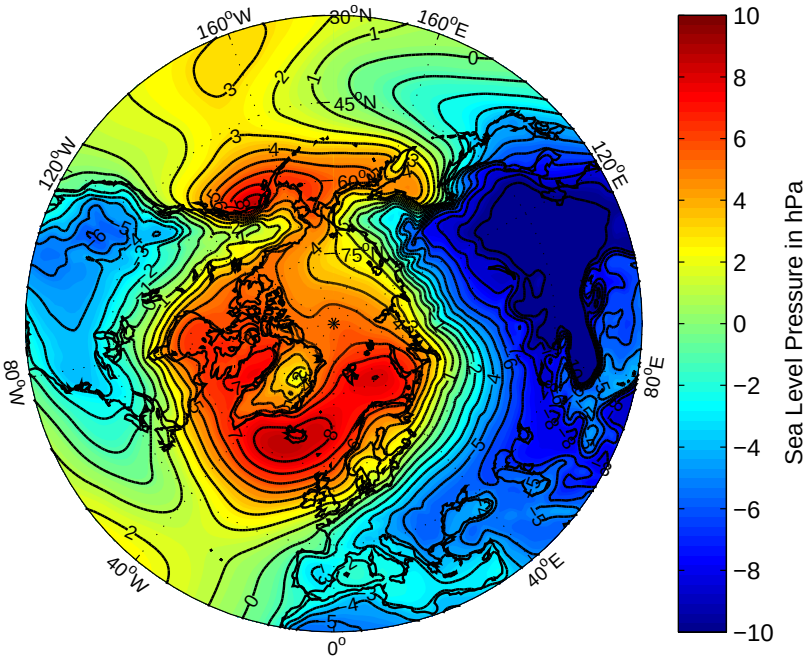

Figure 9: *Seal Level Pressure in hPa. Difference: Spring (55 % Apr/45 % May) minus Autumn (55 % Oct/45 % Nov). Isobars separated by 1 hPa.*

3.2.1 Surface Flow

In Figure 9 the spring-autumn difference in sea level pressure (SLP) is depicted. Even though frictional effects prevent the flow in the boundary layer from being properly geostrophic, the isobars are still good indicators for the surface wind direction. The ageostrophic component depends on the surface roughness but is generally small and

oriented left to the geostrophic flow.

Firstly, it can be observed that SLP is lower on the continents and higher over the oceans in spring relative to autumn. This can primarily be attributed to inverted land-ocean heating contrasts in the transition seasons. Secondly, positive values occur in the Arctic, whereas at midlatitudes negative differences prevail (autumn SLP higher). This indicates stronger westerlies in autumn especially over the continents. Recalling the annual cycle phase patterns, it is interesting to note that the eastasian coast seems to face more northerly flow in autumn due to the pronounced Siberian High, whereas Northeastern America tends to have more southwesterly influence. The same wind asymmetry prevails over Europe.

Additionally, land-ocean temperature contrasts have to be considered when estimating the impact of the surface circulation in the transition seasons. More warm southerly maritime air is advected over the eastasian coast in spring and cold northerly continental air arrives in autumn. This is consistent with an early annual cycle phase in temperature. In northeastern North America though, northeasterly air flows over the cool Labrador Sea in spring and more influence from the southeastern continent prevails in autumn, which can be connected to a delayed annual cycle. In northern central Russia late phases coincide with this type of seasonal circulation change as well. The situation observed over Europe is a bit ambiguous since there is northeasterly influence from the continents in spring and southwesterly advection from the Atlantic Ocean in autumn. However, the land-sea temperature contrast in autumn can be expected to be less pronounced in this region, so that these circumstances should still tend to delay the temperature annual cycle.

Yet, there are surely limits to this argument and the link between annual cycle phase lag and seasonal changes of surface circulation is for instance not consistent over central and western Canada. Remember that the positive phase anomaly and particularly the delayed autumn extend westward to about 110°W in Figures 4 and 8, where Figure 9 displays surface wind, being more southeasterly in spring-autumn diferrence. Moreover, the situation over Western Canada, facing southerly components in both transition seasons, seems to be rather unclear. It is likely that other factors play an important role for the early annual cycle in this particular region such as seasonal changes in surface albdeo connected to the Rocky Mountains. In addition, it has to be considered that the surface circulation only represents one aspect of the the horizontal atmospheric heat transport. A major contribuation comes from the flow above the boundary layer, as far as horizontal temperature gradients are still pronounced and high geostrophic velocities prevail.

3.2.2 Variability Patterns in Sea Level Pressure

The spring-autumn SLP differences in Figure 9, inducing the discussed asymmetries in surface circulation, can be resolved in a more general context of varaibility patterns by applying EOF-Analysis. It is conducted for monthly SLP anomalies poleward of 20°N over the period from 1979 to 2013 similiar to *Kidson* (1975). It differs from common procedures to capture the Northern Annular Mode (NAM), since the seasonal cycle was not removed from the anomalies. By this means seasonal variability remains in the data and shapes the leading EOFs and their corresponding principal components.

Figure 10 shows the first EOF obtained, accounting for 52% of the total SLP variance, together with its associated time series. It mainly captures the summer-winter contrast of the Siberian and North American Highs to the Icelandic and Aleutian Lows. It is similar to the Cold-Ocean-Warm-Land pattern (COWL), described by e.g. *Wallace et al.* (1996) for surface air temperature. The corresponding time series is dominated by a distinct annual cycle with a maximum in late December, when the pressure differences between these regions with respect to their mean state are most pronounced. The leading EOF shapes the midlatitudes in Figure 9, since it is about one month earlier in phase than the temperature annual cycle, which leads to asymmetries in the transition seasons defined as 55%/45% April/May and October/November. The principal component is already negative in spring and positive in autumn.

The second EOF explains 11% of the variance and can be seen in Figure 11. It closely reproduces the pattern of the NAM with its characteristic oval minimum over the Arctic and the maxima over the Azores High and the Aleutian Low regimes. However, it is not the same as the NAM since the latter is normally derived as the leading EOF of SLP anomalies from monthly climatological means as e.g. in *Thompson and Wallace* (1998) and thus only comprises interannual variability. It appears as the second EOF here though, since the seasonal cycle is not removed from the anomalies. An inspection of the corresponding principal component reveals seasonal as well as interannual variability. The interannual part obviously dominates, exhibiting well-known NAM winter-events such as the maximum in 2007 or minimum in 2010. In addition, an annual component can be found with a maximum in mid-October, explaining about 20% of the time series variance. This mode seems to be responsible for constant spring-autumn asymmetries in atmospheric circulation, especially since it can be found in similar form on mid-tropospheric levels as well.

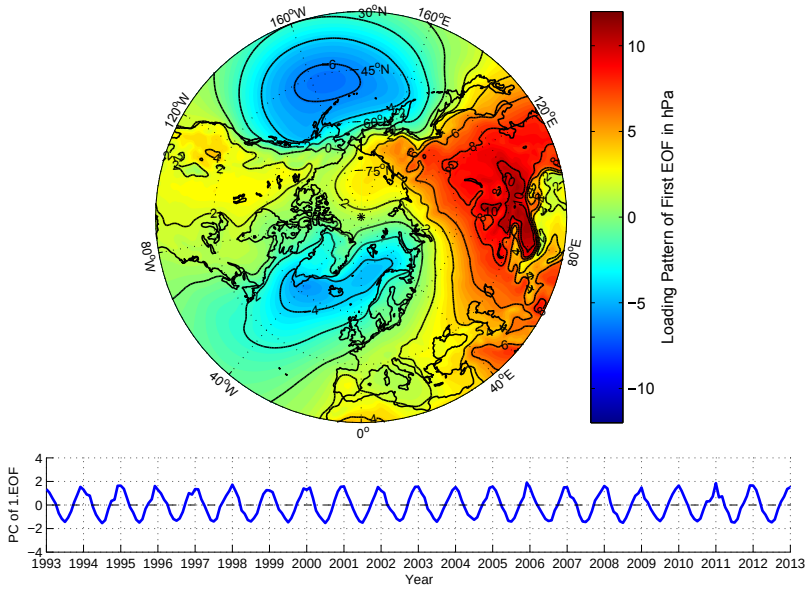

Figure 10: *First EOF of monthly SLP anomalies between 20°N and 90°N over the period from 1979 to 2013 in hPa with corresponding principal component (shown for 1993 to 2013). The anomalies are computed from the climatological mean and therefore still include seasonal variation. The pattern stands for the SLP anomaly produced by a fluctuation of one unit in principal component. This mode explains 52% of the SLP variance. The annual component of the time series has a minimum in late December and explains 96% of the total principal component variance.*

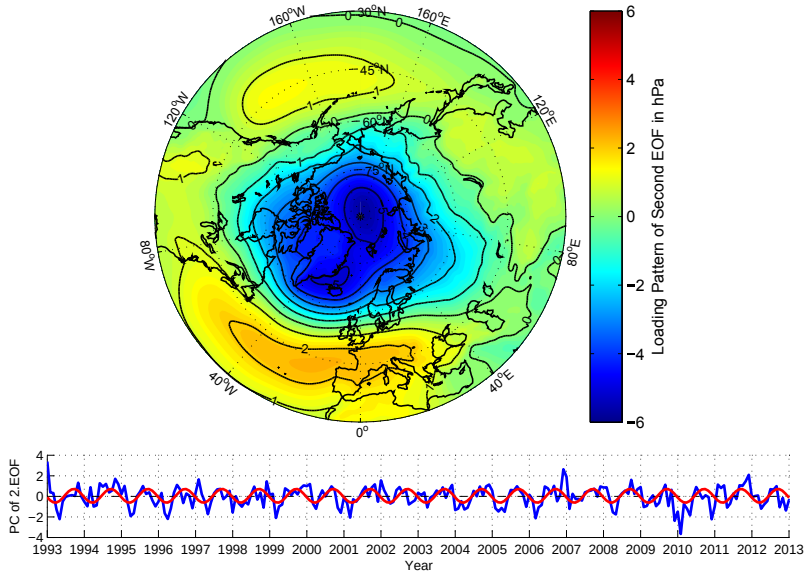

Figure 11: *As in Figure 10 except for the second EOF. Note the different colorbar and the contour interval of 1 hPa. This mode explains 11% of the SLP variance. The annual component (red line) of the time series has a minimum in mid-April and explains 20% of the total principal component variance.*

The spring-autumn difference pattern in Figure 9 can thus mainly be interpreted as an interaction of these first two EOFs, each one of them being in its negative phase. The COWL pattern clearly dominates in mid - and subpolar latitudes. However, although its signal reaches up to high latitudes by producing the Aleutian and Icelandic pressure anomalies, it cannot fully account for the distinct annular structure over the Arctic. This pattern can rather be attributed to the second EOF and its seasonal variation. It constitutes the Arctic low pressure anomalies in autumn that extend rather symmetrically into the midlatitudes at about 90°W and 90°E respectively, inducing the discussed seasonal circulation changes in northeastern and northwestern North America as well as northern central Asia. An important consequence of this second EOF pattern is moreover the increased poleward gradient, procuding enhanced westerlies. An equivalent Analysis for z500 (see appendix 5.4) captures a second EOF with rather similar features, indicating seasonal changes in jet stream strength. This argument becomes crucial when considering spring-autumn differences in mid-tropospheric flow and stationary waves in the following section.

3.2.3 500 hPa flow

Similiar examinations as for the surface flow can be made on the 500 hPa level. Figure 12 presents spring-autumn differences in 500 hPa geopotential height (z500). Given the geostrophy in the middle troposphere, the contours can be interpreted as streamlines. Evidently, land-sea contrasts are of minor importance compared to the meridional component of the flow, when estimating the temperature advection. Positive values occur over the polar region, whereas negative differences (z500 smaller in spring) can be found in the subtropics. This implies an enhancement of the jet stream in autumn relative to spring similiar to the westerly signal on the surface. *Fleming et al.* (1987) found this increased poleward pressure gradient on all levels of the troposphere and most pronounced in the upper part.

The wave structure of the jet stream is of particular interest, when investigating regional circulation changes between spring and autumn. The argument is similiar as for the surface circulation. Regions with a spring-autumn difference in meridional flow can be expected to have deviating annual cycle phases. Figure 12 shows northeastern North America, having a more pronounced southerly component in autumn. On the northwestern margin of the continent the opposite situation is faced. The eastasian coast though, is exposed to northerly flow components in both seasons. Over Europe the same can be observed less pronounced for southerly advection.

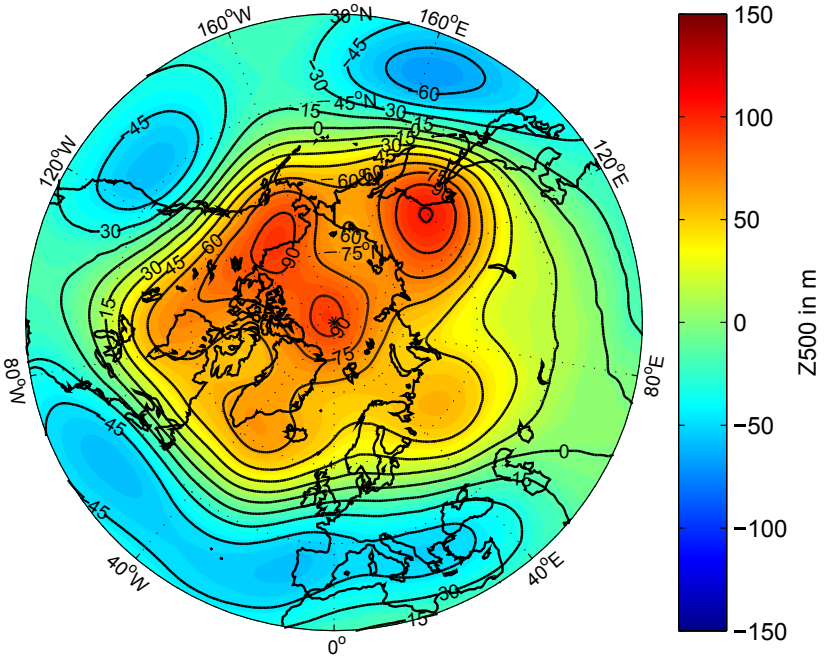

Figure 12: *500 hPa geopotential height (z500) in m. Difference: Spring (55 % Apr/45 % May) minus Autumn (55 % Oct/45 % Nov). Isobars seperated by 15 m.*

The spring-autumn difference pattern in Figure 12 can also be resolved into leading EOFs that include seasonal variability as done for SLP in section 3.2.2 (see appendix 5.4 for corresponding z500 Figures). The second EOF displays an annular structure similar to its equivalent in SLP. Its associated principal component is also characterized by a subtle spring-autumn polarity. The annual component with a minimum in mid-May can explain about 36% of the time series variance. It therefore accounts for an enhancement of the jet stream in autumn relative to spring. This complements the argument made for the second EOF of SLP in section 3.2.2 by showing the existence of this annular mode on mid-tropospheric levels.

Looking at the zonal and meridional components of 500 hPa flow separately in Figures 13 and 14, the character of the spring-autumn differences becomes even more apparent. The jet stream is not only stronger in autumn but also located more northward as Figure 13 indicates. Maximas of longitudinal averaged zonal flow occur at about 38°N in spring and 44°N in autumn. This also agrees with the findings of *Fleming et al.* (1987), who applied the same season definitions. Latitudes with the largest seasonal deviations are between 50°N and 60°N. Since the jet stream is additionally stronger in autumn, there is a negative feature in Figure 13 north of the jet stream maximum, but no positive equivalent south of it. Looking at zonal variation, remarkable seasonal deviations in 500 hPa zonal wind occur at continental margins. In the center of the large Eurasian continent though, the magnitude of the jet stream is widely the same in spring as in autumn. This pattern indicates that land-ocean constrasts in

heating could play an important role for the jet stream enhancement.

Differences in meridional 500 hPa flow between the two transition seasons are displayed in Figure 14. Northeastern North America is dominated by stronger southerly components in autumn (spring and autumn fields were also evalutated separately, not shown here). This manifests itself by negative spring-autumn differences. The situation is different at eastasian midlatitudes, where at the coast the meridional component in autumn is similar to spring and even tends to be more northward inland. At about 160°E increased southerly advection prevails again, which is consistent with delayed annual cycles over northeastern Russia observed in Figures 4 and 7. Over northern and westerm Canada as well as the Taymyr Peninsula in northern Russia however, no such implications for phase lag can be derived from the 500 hPa flow field. Furthermore, Figure 14 presents a wavelike pattern for the spring-autumn differences in meridional mid-tropospheric flow. Five maxima and minima follow each other more or less equally spaced in zonal direction with varying amplitudes, though. This structure is most apparent over the Pacific, eastern Asia and North America.

3.2.4 Stationary Wave Patterns

The zonal structure of the polar jet stream is dominated by planetary stationary waves with ridges over western and troughs over eastern parts of the NH continents. Its forcing is basically due to zonal differences in orography and diabatic heating and is subject to a wide field of research. Essential points are covered by e.g. *Held et al.* (2002). The stationary wave pattern is represented in the following by the z500 zonal anomaly field, shown for spring and autumn in Figures 15 and 16. As *Fleming et al.* (1987) indicated, an enhanced and more northward located jet stream in autumn is likely to produce considerable differences in the stationary wave pattern, since the flow carries more momentum and faces different geographical and orographical conditions. It is well-known that the zonal land-sea distribution mainly determines the diabatic forcing of the stationary waves. In addition, the meridional position of the jet stream is for instance important for the impact of the Tibetian Plateau on the flow. However, with respect to purposes of this study, differences in stationary wave patterns are presented without considering their forcings in further detail. In Figures 15 and 16 it is noticeable that the stationary wave ridges and troughs have more pronounced southwestward extensions in autumn than in spring. Furthermore, their centers are shifted more to the west and are slightly higher in amplitude.

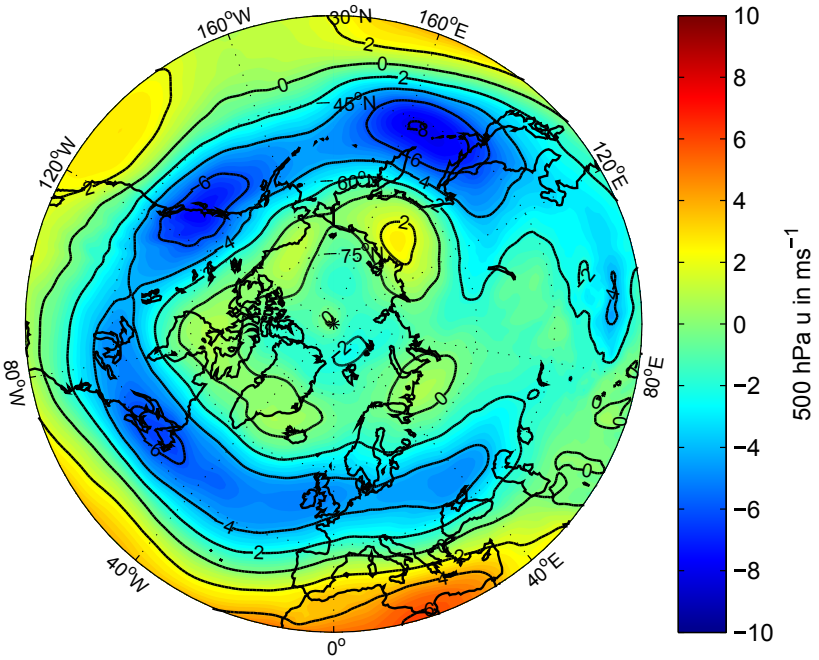

Figure 13: *500 hPa zonal flow in ms^{-1} based on Era-Interim data. Difference: Spring (55 % Apr/45 % May) minus Autumn (55 % Oct/45 % Nov). Contours at 2 ms^{-1}.*

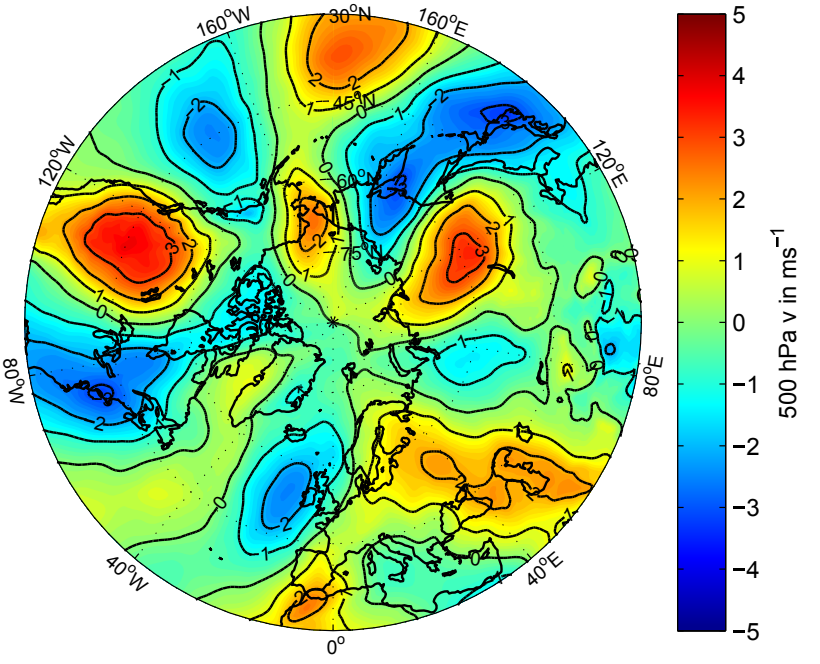

Figure 14: *As in Figure 13 except for meridional flow. Note the different colorbar and the contour interval of 1 ms^{-1}.*

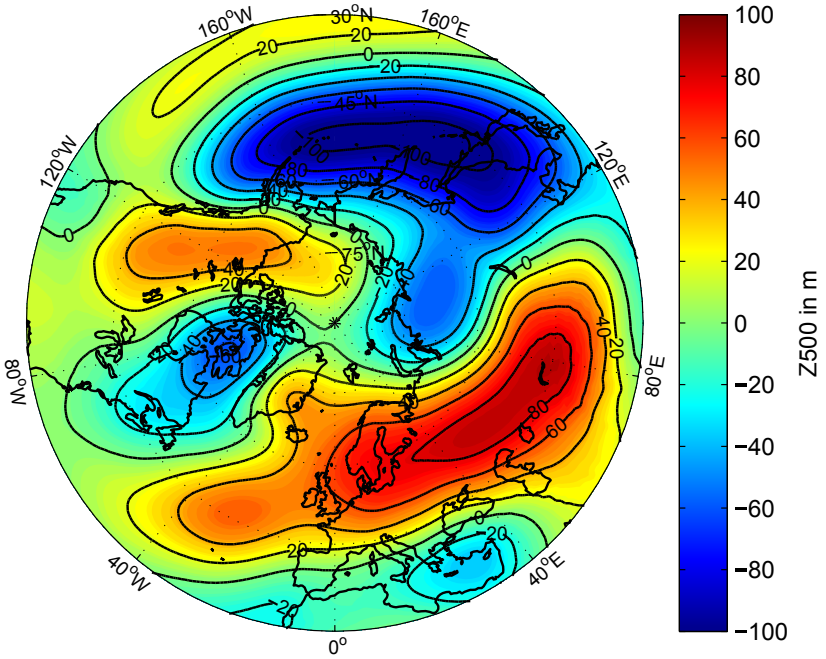

Figure 15: *Zonal Anomaly in 500 hPa geopotential height in m based on Era-Interim data for spring (55 % Apr/45 % May).*

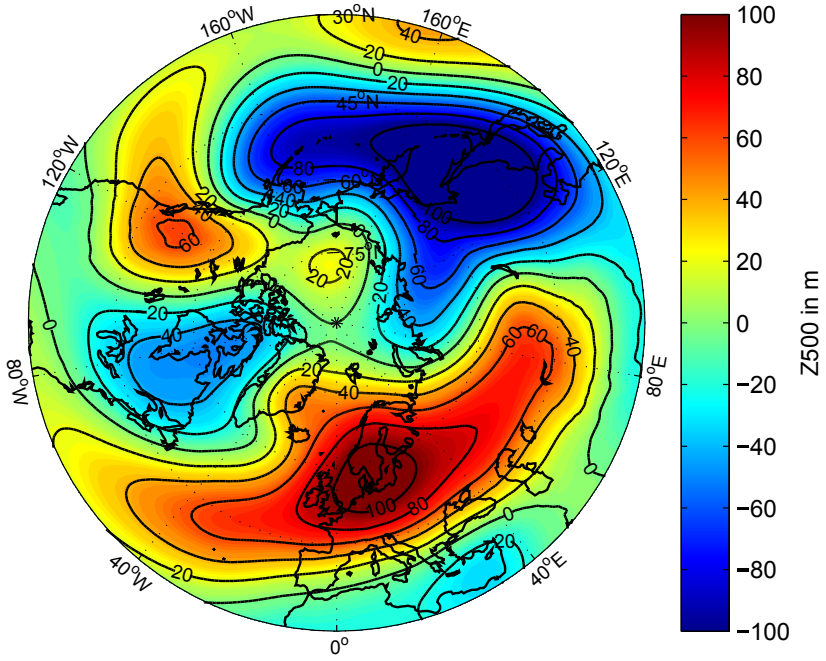

Figure 16: *As in Figure 15 except for autumn (55 % Oct/45 % Nov).*

This has two interesting implications. Firstly, it is basically consistent with the seasonal 500 hPa circulation changes described in 3.2.3. Yet, concerning the two eastern continental margins, it is still important to note that the stationary wave shifts do not have the same consequences: In east Asia the northerly component is enhanced in autumn, whereas over northeastern North America southerly influence is strenghtened as Figure 14 indicates. This is due to the North American trough, shifting more inside the continent, while the Pacific trough is still centered on the continental margin.

Secondly, the southwestward extensions lead to a more anticyclonically tilted shape of the wave pattern in autumn. This is connected to increased average northward transport of westerly momentum. It is defined by $\langle u'v' \rangle$, wherein $\langle u \rangle$ denotes the zonal mean and u' the zonal anomaly of the velocity field. The zonally averaged westerly momentum tendency due to the structure of the stationary waves is given by

$$\frac{\partial \langle u \rangle}{\partial t} = -\frac{\partial}{\partial y} \langle u'v' \rangle \tag{2}$$

and can be seen in Figure 17 for the NH latitudes poleward of 30°N. It shows that the stationary wave momentum flux between 45°N and 65°N is generally enhanced in autumn. Moreover, the maximum is shifted northward by about 4° in latitude. The largest differences occur between 50°N and 60°N, which is consistent with the observed displacement of the jet stream in Figure 13.

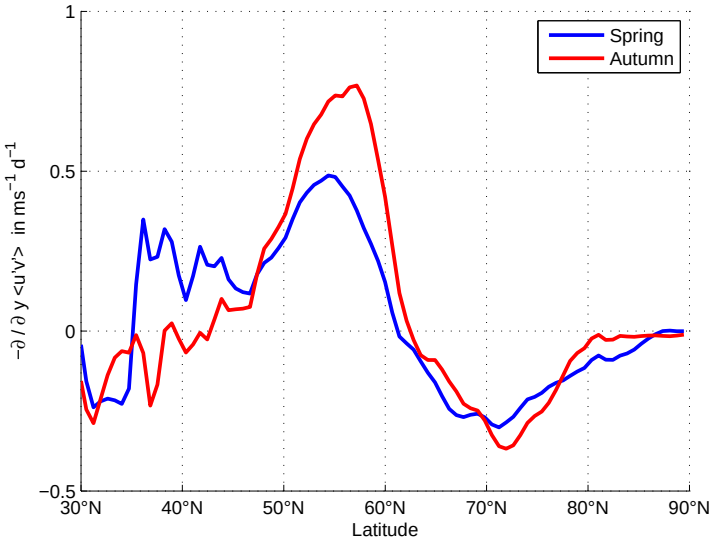

Figure 17: *Zonally averaged flux of westerly momentum by stationary waves according to (2) in $ms^{-1}d^{-1}$ for latitudes poleward of 30°N.*

The spring-autumn contrasts in stationary wave structure and jet stream strenght as well as location have to be considered as two coupled mechanisms. It is likely that the jet stream, hitting meridional mountain chains with more momentum at different

latitudes, produces a different stationary wave pattern. The observed autumn pattern with the southwestward extensions in Figure 16 however also increases the northward flux of westerly momentum, leading to further intensification and northward displacement of the jet stream. Both processes might reinforce each other, building up this specific autumn circulation pattern. Yet, there has to be a trigger for this mechanism, originating in a general asymmetric forcing of the circulation in the two transition seasons.

4 Summary and Discussion

The investigation presented here showed the existence of several regional patterns in temperature seasonality in the extratropical northern hemisphere (NH). Besides the dominating contrast of continental and maritime influence on seasonal timing and annual range, anomalous patterns of annual cycle phase can be identified over northern North America and Asia. The most pronounced signal appears over northeastern North America, where a delayed annual cycle is found in some continental regions, including large parts of Canada east of the Rocky Mountains. A similiar feature is indicated in northern central Russia. Both regions do not show small annual cycle amplitudes as typical for maritime climates. On the other hand relatively small amplitudes are connected with an early annual cycle over northwestern North America. These regions deviate from the characteristic pattern of land-sea contrasts in seasonality. An approach to trace these anomalies is pursued by exploring circulation asymmetries in the transition seasons.

Examining surface and 500 hPa circulation patterns reveals considerable differences between spring and autumn, that are mostly consistent with the indicated phase anomalies of the temperature annual cycle. Northeastern North America is exposed to more northeasterly influence in spring and enhanced southwesterly influence in autumn. Similar changes in meridional flow are observed over northwestern North America (enhanced northerly component in autumn) and northern central Asia (enhanced southerly component in spring), yet only in surface flow for the latter.

Spatial patterns of SLP variability in the extratropical NH are obtained by EOF-Analysis that give further insight into the seasonal variation of the surface circulation. The first mode accounts for the annual cycle in pressure difference between the Siberian and North American high regimes and the Icelandic and Aleutian low regimes. It reflects land-ocean contrasts in heating and is referred to as the Cold-Ocean-Warm-Land-pattern (COWL) according to *Wallace et al.* (1996). The phase of this mode is about one month earlier than the mean temperature annual cycle, implying asymmetries in surface circulation between spring and autumn. However, a second EOF is found, which is similiar to the well-known Northern Annular Mode (NAM), but also includes seasonal variation, that indicates a considerable spring-autumn polarity. This second pattern is particularly interesting because it can be similarly reproduced on the 500 hPa level, accounting for an enhanced jet stream in autumn. In fact, comparison of 500 hPa stationary wave patterns, zonal wind and momentum flux furthermore shows evidence for a stronger jet stream in autumn relative to spring that is located more northward. The spring-autumn asymmetries in jet stream strength and position are likely to produce different orographically induced stationary wave patterns that might

finally account for the discussed shifts in circulation. These results overall confirm the findings of *Fleming et al.* (1987), who investigated circulation differences between the transition seasons in further detail. The study presented here collected evidence from reanalysis data for these seasonal asymmetries, being responsible for anomalous patterns in the delay of the temperature annual cycle. A convincing demonstration of this relation though, would require a more quantitative evaluation of the impact of seasonal circulation changes on the annual cycle such as provided by general circulation modeling experiments.

The analysis of temperature seasonality is focused on the annual cycle. However, in some regions the semi-annual cycle or even higher harmonics have to be considered to obtain a more comprehensive picture of seasonal variations. It has to be questioned as well to what extent differences in annual cycle amplitude or phase might only be artefacts of harmonic analysis, if considerable variance originates from the semi-annual component. It would be useful to derive a criterion for typical daily climatologies, estimating the minimum variation in amplitude and phase that is significant, given a certain percentage of variance explained by the annual cycle. Moreover, to confirm some smaller regional features of delayed annual cycle such as over the subpolar Asian continent, more station data would have to be analysed.

The examination of seasonal circulation changes was closely related to the study of *Fleming et al.* (1987). Transition seasons defined by similar tropospheric mean temperature were compared based on the reasoning that the annual cycle is steepest during these periods. Asymmetrical influence during the seasons is supposed to produce the largest impact on phase delays. However, as the COWL pattern obtained by EOF-Analysis indicated, it only needs a constant phase delay relative to the temperature annual cyle to create asymmetric circulation effects. In genereal, any forcing with an annual period and deviating phase would be able to generate those phase shifts. Against this background the applied definitions of the transition seasons (55%/45% April/May and October/November) appear a bit arbitrary since the responsible forcing does not necessarily need to have a corresponding spring-autumn polarity. It would also be interesting to compare transition periods based on different definitions such as late winter/summer or early spring/autumn. Many of the presented comparisons were sensitive to subtle changes in the definition of spring and autumn.

The exploration of the mechanisms that cause the observed asymmetries in surface and mid-tropospheric circulation, are beyond the scope of this study. It is not clear how to interpret the COWL variation, being more than one month in advance of the temperature annual cycle. Not to mention the other EOFs for SLP and z500, which are presented primarily as statistical features here. A physical explanation suggested

for the spring-autumn differences in 500 hPa flow was the variation in jet stream strength and position. It would be interesting to learn from modeling experiments to what extent this accounts for the southwestward extensions of the stationary waves in autumn. It was speculated that both processes might reinforce each other to some degree, gradually constructing a different circulation regime in autumn. Yet, this still requires a trigger to initiate the mechanism, that must be based on some fundamental asymmetry in the two transition seasons. A possible candidate would be the land-ocean temperature contrast. It is known to play an important role for the diabiatic forcing of the stationary waves. *Fleming et al.* (1987) furthermore suggested a connection to the tropical convection that shows considerable zonal asymmetries in spring and autumn. Sure enough, several paths can be followed to trace the origin of the discussed patterns in spring-autumn circulation differences. This study primarily intended to track those differences, in order to provide an explanation for regional anomalies found in the seasonality of surface temperature over the northern hemisphere.

5 Appendix

5.1 Station Data

This section provides details on the daily station data used. The data are either obtained from the Global Historical Climatology Network of the National Climatic Data Center (NCDC), the Carbon Dioxide Information and Analysis Center at Oak Ridge (CDIAC) based on data collection by *Bulygina and Razuvaev* (2012) or the European Climate Assessment & Dataset project (ECAD). The percentage of data missing (PDM) refers to the analysed period from 1959 to 2009. The temperature measure (TM) used is either the daily mean temperature (Mean) or the average of daily maximum and minimum temperature (MinMax). The explained variance (ExpVar) refers to the annual component of the seasonal cycle.

Station Name (State), Country	Location	Source	TM	PDM	ExpVar
Aberdeen (Saskatchewan), Canada	$123.7°W, 47.3°N$	NCDC	Mean	1.3 %	97.0 %
Annapolis (Nova Scotia), Canada	$65.5°W, 44.7°N$	NCDC	MinMax	1.1 %	99.1 %
Brochet (Manitoba), Canada	$101.7°W, 57.9°N$	NCDC	MinMax	9.6 %	99.2 %
Goose Bay (Labrador), Canada	$60.4°W, 53.3°N$	NCDC	MinMax	0 %	98.8 %
Kuujjuak (Quebec), Canada	$68.4°W, 58.1°N$	NCDC	MinMax	0.1 %	98.9 %
Kuujuarapik (Quebec), Canada	$77.7°W, 55.2°N$	NCDC	MinMax	0.5 %	97.4 %
Valcartier (Quebec), Canada	$71.5°W, 46.9°N$	NCDC	MinMax	0.4 %	98.2 %
Arborg (Manitoba), Canada	$97.1°W, 50.1°N$	NCDC	MinMax	1.3 %	98.4 %
Churchill (Manitoba), Canada	$94.1°W, 58.8°N$	NCDC	MinMax	0.1 %	99.5 %
Sheenboro (Ontario), Canada	$77.2°W, 46.0°N$	NCDC	MinMax	2.6 %	98.3 %
Kapuskasing (Ontario), Canada	$82.5°W, 49.4°N$	NCDC	MinMax	0.3 %	98.4 %
St John's (Newfoundland), Canada	$52.8°W, 47.6°N$	NCDC	MinMax	0 %	98.6 %
Halifax (Nova Scotia), Canada	$63.6°W, 44.6°N$	NCDC	MinMax	0.5 %	99.2 %
Anette Island (Alaska), USA	$131.6°W, 55.0°N$	NCDC	MinMax	0 %	97.7 %
Barkerville (British Columbia), Canada	$121.5°W, 53.1°N$	NCDC	MinMax	1.0 %	98.1 %
Bayview (Montana), USA	$116.6°W, 48.0°N$	NCDC	Mean	0.7 %	96.8 %
San Francisco Oceanside (California), USA	$122.5°W, 37.7°N$	NCDC	Mean	0.6 %	81.2 %
Vancouver (British Columbia), Canada	$123.2°W, 49.2°N$	NCDC	MinMax	0 %	97.8 %
Danmarkshavn, Denmark (Greenland)	$18.6°W, 76.7°N$	ECAD	Mean	7.0 %	95.5 %
Hatanga, Russia	$102.5°E, 72.0°N$	ECAD	Mean	0 %	97.9 %
Hamburg Fuhlsbuettel, Germany	$10.0°E, 53.6°N$	ECAD	Mean	0.1 %	99.2 %
Ica, Russia	$155.5°E, 55.6°N$	ECAD	Mean	4.4 %	99.2 %
Saskylah, Russia	$114.1°E, 72.0°N$	ECAD	Mean	3.3 %	98.2 %
Sevilla San Pablo, Spain	$5.9°W, 37.5°N$	ECAD	Mean	0.4 %	97.3 %
Stockholm, Sveden	$18.0°E, 59.4°N$	ECAD	Mean	0 %	98.8 %
St Peterburg, Russia	$30.3°E, 60.0°N$	ECAD	Mean	5.9 %	99.3 %
Stykkisholmur, Iceland	$22.6°W, 65.1°N$	ECAD	Mean	8.6 %	96.7 %
Uralsk, Kazakhstan	$51.5°E, 51.2°N$	ECAD	Mean	7.9 %	98.6 %
La Rochelle, France	$1.1°W, 46.1°N$	ECAD	Mean	9.8 %	98.2 %
Pogibi, Russia	$141.6°E, 52.2°N$	CDIAC	Mean	3.0 %	98.5 %
Ohotsk, Russia	$137.6°E, 59.6°N$	CDIAC	Mean	0.4 %	97.9 %
Poliny Osipenko, Russia	$136.5°E, 52.4°N$	CDIAC	Mean	0 %	97.9 %
Sovetskaja Gavan, Russia	$140.3°E, 49.0°N$	CDIAC	Mean	1.2 %	97.2 %
Ust Maja, Russia	$134.5°E, 60.4°N$	CDIAC	Mean	0.2 %	98.6 %
Vladivostok, Russia	$131.9°E, 43.8°N$	CDIAC	Mean	2.0 %	96.3 %
Bogorodskoe, Russia	$140.5°E, 52.4°N$	CDIAC	Mean	1.2 %	98.4 %
Arhara, Russia	$130.0°E, 49.5°N$	CDIAC	Mean	0.1 %	98.1 %
Bajkit, Russia	$96.3°E, 61.6°N$	CDIAC	Mean	0.4 %	98.7 %
Esso, Russia	$158.6°E, 57.7°N$	CDIAC	Mean	2.9 %	99.5 %
Golomjannyj, Russia	$90.8°E, 79.4°N$	CDIAC	Mean	8.9 %	98.0 %
Korf, Russia	$166.6°E, 60.3°N$	CDIAC	Mean	2.9 %	98.1 %
Kotlas, Russia	$46.6°E, 61.2°N$	CDIAC	Mean	0 %	99.3 %
Nenastnaja, Russia	$88.9°E, 54.8°N$	CDIAC	Mean	1.5 %	98.9 %
Volochanka, Russia	$94.5°E, 71.0°N$	CDIAC	Mean	0.9 %	97.6 %
Frankfurt Airport, Germany	$8.5°E, 50.0°N$	ECAD	Mean	0%	99.2 %
Oslo Blindern, Norway	$10.6°E, 60.0°N$	ECAD	Mean	9.8 %	99.4 %

Table 1: *Station Name, Location, Source, Temperature Measure (TM) and Percentage of Data Missing in 1959 to 2009 (PDM) for the daily temperature station data used. The explained variance (ExpVar) refers to the annual harmonic fit to the seasonal cycle.*

5.2 Semi-Annual Cycle

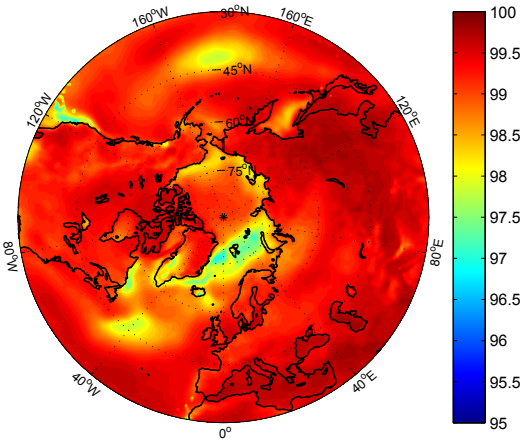

Figure 18: *Percentage of variance of seasonal cycle explained by annual and semi-Annual Cycle together in %. The seasonal cycle is a daily climatology of 2m-air-temperature ERA-Interim data over 1979 to 2013.*

5.3 Annual Cycle Amplitude

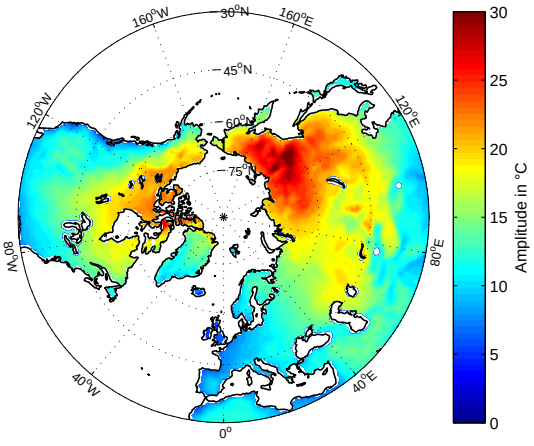

Figure 19: *2m-air-temperature annual cycle amplitude A in °C for land areas on the extratropical NH base on daily ERA-Interim data from 1979 to 2013. The difference to Figure 3 is that no latitudal weighting was applied to remove the imapct of the meridionally increasing solar insolation amplitude.*

5.4 EOF-Analysis for 500 hPa geopotential height

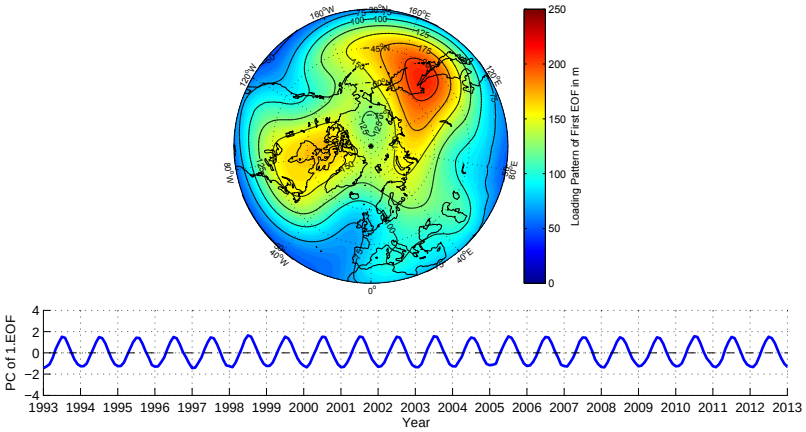

Figure 20: *First EOF of monthly z500 anomalies between 20°N and 90°N over the period from 1979 to 2013 in m with correponding principal component (shown for 1993 to 2013). Note the colorbar, all anoamalies develop in the same direction over time. The anomalies are based on monthly ERA-Interim data computed as departures from the climatological mean and therefore still include seasonal variation. The pattern stands for the z500 anomaly produced by a flucuation of one unit in principal component. This mode explains 67% of the z500 variance. The annual component of the time series has minimums in late December and explains 96% of the principal component variance.*

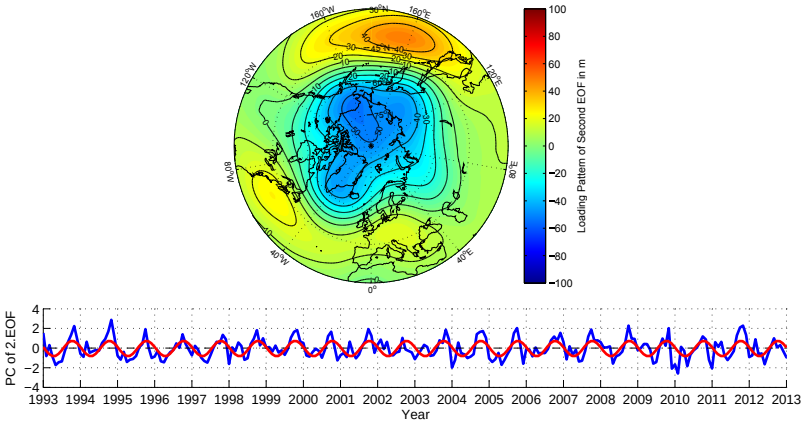

Figure 21: *As in Figure 20 except for the second EOF. Note the different colorbar and the contour interval of 10 m. This mode explains 3% of the z500 variance. The annual component (red line) of the time series has minimums in mid-May and explains 34% of the principal component variance.*

References

Bjornsson, H., and S. Venegas (1997), A manual for EOF and SVD analyses of climatic data, *CCGCR Report*.

Bulygina, O. N., and V. N. Razuvaev (2012), Daily Temperature and Precipitation Data for 518 Russian Meteorological Stations, Carbon Dioxide Information Analysis Center, Oak Ridge National Laboratory, U.S. Department of Energy, Oak Ridge, Tennessee, doi:10.3334/CDIAC/cli.100.

Fleming, E. L., L. Gyu-Ho, and J. M. Wallace (1987), Differences between the spring and autumn circulation of the Northern Hemisphere, *Journal of the Atmospheric Sciences*, *44*, 1266–1286.

Hannachi, A., and I. Jolliffe (2006), In search of simple structures in climate: simplifying EOFs, *International Journal of Climatology*, *26*(1), 7–28.

Held, I. M., M. Ting, and H. Wang (2002), Northern winter stationary waves: theory and modeling, *Journal of Climate*, *15*, 2125–2144.

Jaagus, J., and R. Ahas (2000), Space-time variations of climatic seasons and their correlation with the phenological development of nature in Estonia, *Climate Research*, *15*(15), 207–219.

Kendrew, W. G. (1927), *The Climates of the Continents*, 13–17 pp., Claredon Press.

Kidson, J. (1975), Eigenvector analysis of monthly mean surface data, *Monthly Weather Review*, *103*, 177–186.

McHall, Y. L. (1991), Planetary stationary waves in the atmosphere Part I: Orographic stationary waves, *Advances in Atmospheric Sciences*, *8*(2), 211–224.

Prescott, J. A., and J. A. Collins (1951), The lag of temperature behind solar radiation, *Quarterly Journal of the Royal Meteorological Society*, *77*(331), 121–126.

Schwartz, M. D., R. Ahas, and A. Aasa (2006), Onset of spring starting earlier across the Northern Hemisphere, *Global Change Biology*, *12*(2), 343–351.

Stine, A. R., P. Huybers, and I. Y. Fung (2009), Changes in the phase of the annual cycle of surface temperature., *Nature*, *457*(7228), 435–441.

Thompson, D. W. J., and J. M. Wallace (1998), The Arctic Oscillation signature in the wintertime geopotential height and temperature fields, *Geophysical Research Letters*, *25*(9), 1297–1300.

Wallace, J. M., Y. Zhang, and L. Bajuk (1996), Interpretation of interdecadal trends in Northern Hemisphere surface air temperature, *Journal of Climate*, *9*, 249–259.

White, G. H., and J. M. Wallace (1978), The global distribution of the annual and semiannual cycles in surface temperature, *Monthly Weather Review*, *106*, 901–906.

Selbstständigkeitserklärung

Hiermit erkläre ich, dass ich meine Bachelorarbeit mit dem Titel *On regional differences in the seasonality of northern hemisphere temperature* selbständig und ohne Benutzung anderer als der angegebenen Hilfsmittel angefertigt habe und dass ich alle Stellen, die ich wörtlich oder sinngemäß aus Veröffentlichungen entnommen habe, als solche kenntlich gemacht habe. Die Arbeit hat bisher in gleicher oder ähnlicher Form oder auszugsweise noch keiner Prüfungsbehörde vorgelegen.

Ich versichere, dass die eingereichte schriftliche Fassung der auf dem beigefügten Medium gespeicherten Fassung entspricht.

Kiel, 14.07.2014